JOURNAL OF MATERIALS SCIENCE **35** (2000) 3459–3466

Engineering magnetic nanocomposite microstructures

D. J. BRANAGAN*
Lockheed Martin Idaho Technologies Company, Idaho National Engineering and Environmental Laboratory, P.O. Box 1625, Idaho Falls, ID 83415-2218, USA
E-mail: brandj@inel.gov

M. J. KRAMER, YALI TANG, R. W. McCALLUM
Ames Laboratory, Iowa State University, Ames, IA 50011, USA

D. C. CREW, L. H. LEWIS
Department of Applied Science, Brookhaven National Laboratory, Upton, NY 11973, USA

The realization of high energy densities in permanent magnetic materials requires careful control of both the composition and the processing conditions to develop appropriate microstructures. In this paper, we will show that manipulation of multiple alloying additions leads to the synthesis of magnetically optimum nanoscale metal matrix composite microstructures in a 9-element modified Nd-Fe-B alloy. The development of composite microstructures in hard magnetic materials is a novel concept resulting in many beneficial effects on the resulting structure/processing/property relationships.

1. Introduction

Permanent magnets based on the $Nd_2Fe_{14}B$ phase are a commercially important part of a multibillion dollar industry. This phase has excellent room temperature intrinsic properties which include a high magnetization (16,200 G) [1] along with a high uniaxial anisotropy field (7.3 T) [2]. Commercially, magnets are made from this material through two different routes, either by a press/sinter powder metallurgy approach or by rapid solidification using melt-spinning. Currently, the majority of the Nd-Fe-B magnets are of the sintered type but there has been a trend to find alternatives due to its high processing cost. Isotropic bonded magnets, which are formed by mixing the rapidly solidified material with epoxy, are a lower cost alternative and represent the largest growing market segment. Injection molding techniques allow near net shape magnets or magnet assemblies with complex geometries to be easily fabricated with multipole configurations at the surface. Current and expanding applications for bonded Nd-Fe-B magnets would include such devices as printer stepper motors, hard disk drives, air bag sensors, hybrid generators, transmission solenoids, CD ROM, and DC power tools.

While the $Nd_2Fe_{14}B$ phase has excellent intrinsic magnetic properties, the hard magnetic properties of permanent magnets containing this phase depend very sensitively on the microstructure. Only by developing specific microstructures can significant amounts of magnetic field energy be stored in the magnetic material to make it permanent. The figure of merit commonly used to describe how much energy is stored in a hard magnetic material is called the energy product and is proportional to the largest rectangle in the second quadrant of the demagnetization curve. To develop an optimum isotropic Nd-Fe-B magnet, the amount of hard magnetic phase must be maximized since in the isotropic state, the remanent magnetization will be reduced by half from the saturation value [3]. This condition implies that the amount of grain boundary phases must be minimized in order to maximize the reduced magnetization. In order to achieve significant coercivity without magnetically insulating grain boundary phases, the grain size must be very small. By reducing the grain size below the single domain diameter (0.3 μm for $Nd_2Fe_{14}B$), each grain will contain a single domain in the absence of an externally applied field [4]. The grain boundaries will be concurrent with and will pin the domain wall boundaries allowing high resistance to demagnetization; i.e. high coercivity.

The ability to alter and control microstructural development during solidification is key to the development of favorable microstructures. This goal can be acheived by either changing the processing conditions, which can only be varied over practical limits, or by altering the composition, which can detrimentally effect the hard magnetic properties. A conventional approach toward alloy design would rely on alteration of the intrinsic properties of the magnetic phase whereby single element additions are added to the target alloy and the resulting changes in properties are measured. Even in the best cases where a certain property can be improved,

* Author to whom all correspondence should be addressed.

it comes at the price of reducing (degrading) another. Often, any beneficial effects on the microstructure resulting from solidification are offset by detrimental reductions in the intrinsic magnetic properties.

In this paper, we will show how we can develop desirable hard magnetic properties through the manipulation and control of multiple elemental additions to the base Nd-Fe-B alloy. The focus of this paper will be both on the pathway of developing composite microstructures and the resulting beneficial effects of this approach. Three stages of metal matrix composite development will be described which includes; the dissolution of the elements into the liquid melt, the rapid solidification of the liquid melt to incorporate the alloying elements into the metallic glass, and the devitrification of the metallic glass to yield a multiphase nanoscale composite microstructure.

2. Experimental procedure

In order to emphasize the various roles of the alloying elements, a nine element alloy (Alloy COMP) was developed with the following composition (wt%); 14.8 Nd, 9.9 Pr, 3.0 Dy, 60.2 Fe, 6.9 Co, 1.2 B, 2.4 Ti, 0.8 Zr, 0.8 C. To illustrate the effects of the additions, results obtained on the COMP alloy will be compared to those obtained from the ternary stoichiometric Nd-Fe-B alloy (26.7 wt% Nd, 72.3 wt% Fe, and 1.0 wt% B). Ingots for melt-spinning were formed from high purity elements by arc-melting in ultra high purity (UHP) argon. Melt-spinning was performed in UHP argon on a copper chill wheel with varying tangential wheel velocities while other processing parameters (i.e., superheat temperature, ejection pressure, ejection temperature etc.) were held as constant as possible to give uniform and reproducible cooling rates. Inert gas atomization was done on an 8 lb. melt using a close coupled annular gas atomizer and involves impinging a high velocity gas jet onto a aspirated liquid melt stream. A Gaussian distribution of spherical powder particles was produced from submicron to 150 μm range in size with a mean diameter of 30 μm. The optimum vacuum (5×10^{-6} torr) heat treatment for both alloys was found to be 800°C for 10 minutes. The magnetic properties were measured with a Lakeshore Vibrating Sample Magnetometer (VSM) which had a maximum applied field of 2.3 T. Prior to magnetization measurements, the samples were pulse magnetized in a 3.5 Tesla field. No demagnetization corrections were used for the magnetic measurements and a density of 7.6 g/cm^3 was used to calculate the magnetization. X-ray diffraction was performed on powdered samples after incorporation of a silicon standard using a Philips X-ray Diffractometer with filtered Cu-K_α radiation. Rietveldt analysis was performed with SIROQUANT software and the patterns were refined until a good fit was achieved (total Chi-Squared < 3.0).

3. Results and discussion

3.1. Alloy design

When alloying elements are added to the base material, these elements can interact in several different ways: (1) the added elements may not react at all and may form immiscible liquids, (2) the added elements can selectively dissolve in one of the phases in the host material, (3) the added elements can react with the constituents of the host material to form new phases and/or (4) the added elements can react with each other to form separate phases. In general, in the development of optimal magnetic composites only type 4 alloying behavior is desirable although type 2 behavior is acceptable for a limited number of beneficial intrinsic additions. Since the $Nd_2Fe_{14}B$ phase is a true ternary phase, the achievement of successful microstructures is difficult due to the dissimilar nature of the constituent elements and their varied individual reactivities.

The elements comprising the COMP alloy can be divided up into three categories: base elements (Nd, Fe, and B), intrinsic additions (Pr, Dy, and Co), and extrinsic additions (Ti, Zr, and C). The base elements are the constituent elements of the hard magnetic phase. The intrinsic additions exhibit type 2 behavior and when alloyed alone are known to substitutionally dissolve into the $Nd_2Fe_{14}B$ phase resulting in beneficial modifications of specific intrinsic magnetic properties [5–8]. The extrinsic additions exhibit type 4 behavior and are known to react with each other to form separate transition metal carbides [9, 10]. The important point to consider is that all of the additions, when they are dissolved in the liquid melt, alter solidification. Titanium and zirconium additions have been previously shown to be extremely effective in increasing glass forming ability of Nd-Fe-B melts [9, 10]. The additional alloying elements should also increase glass forming ability since multi-component mixtures have multiple atomic diameters which stabilize molecular associations in the glass structure [11]. The additional alloying elements change the 2-14-1 from a line compound to a solid solution. In this case the composition of the solid is different from that of the liquid with which it is in equilibrium. The results in a build-up of a compositional gradient ahead of the solidification front. The gradient must equilibrate by diffusion before the front can advance. This reduces the velocity of the front and is referred to as solute drag. Clearly, it is easier to obtain a large amorphous fraction in a material with a slow moving solidification front.

3.2. Pathway toward composite formation

3.2.1. Liquid melt dissolution

In order for the alloying elements to have potential value, they must be soluble in the liquid melt which means that immiscible liquids must not form or liquid solubility limits at the superheat temperature (≈1500°C) should not be exceeded. One way to examine the solubility of a given element in a compound is to cast an ingot at the target composition and directly observe the microstructure. The as-cast structure of the COMP alloy is shown in Fig. 1a. Multiple phases are present in the as-cast ingot which are expected due to the nonequilibrium peritectic solidification sequence [12]. Throughout the cross section, bulk phase separation indicating immiscibility is not observed. However, 10 μm cubic shaped precipitates identified by EDS analysis

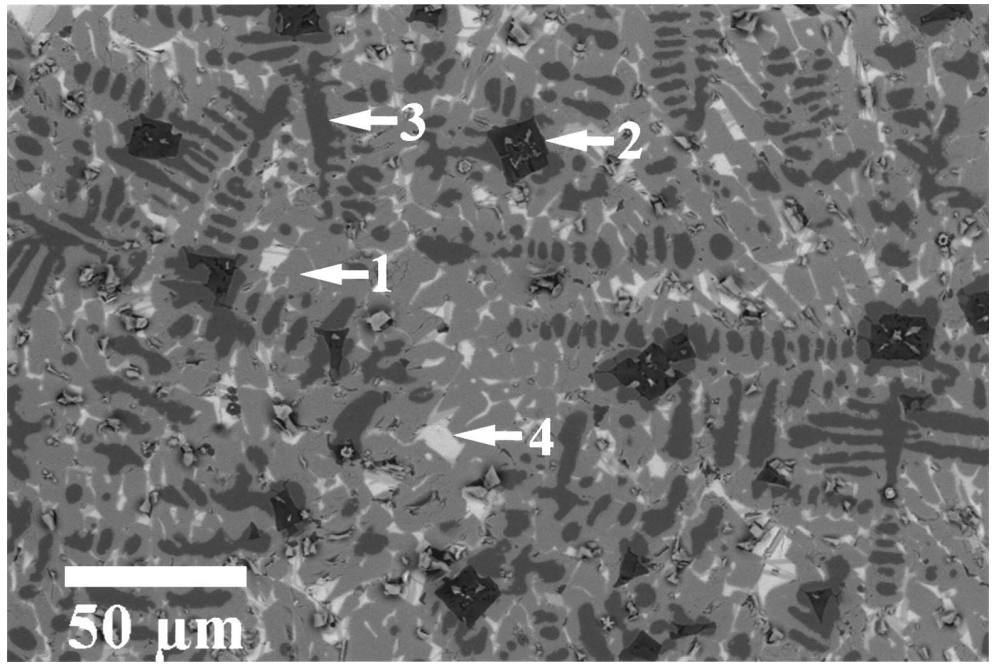

(a)

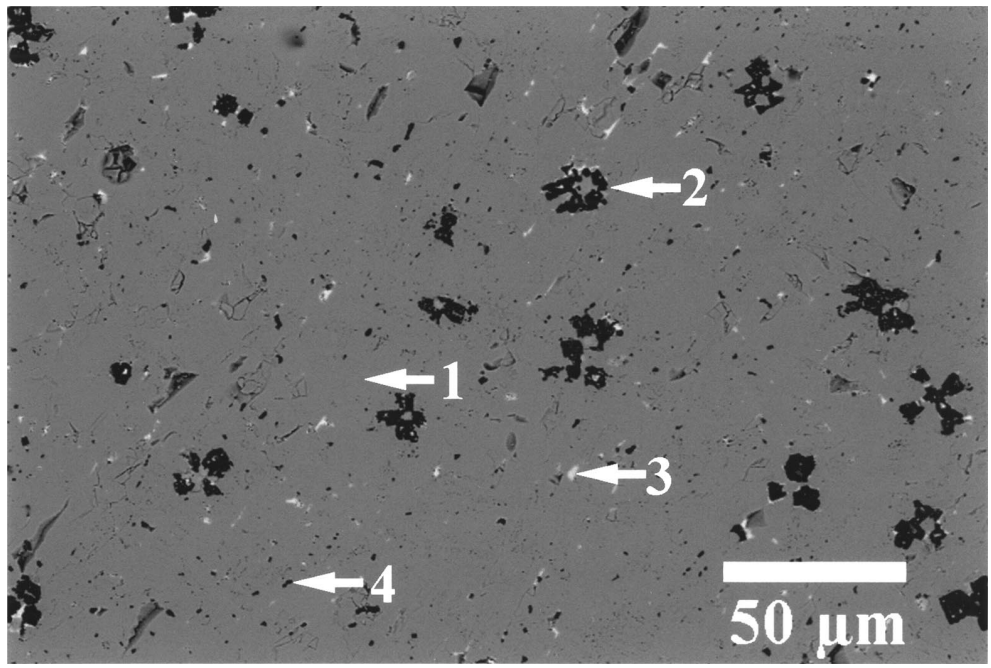

(b)

Figure 1 Backscattered electron images of ingots of the COMP alloy. (a) As-cast ingot with the following phases: (1) $Nd_2Fe_{14}B$, (2) primary TiC, (3) α-Fe, (4) unresolved rare earth rich eutectic phase. (b) Homogenized ingot (1050°C for 24 hours) with the following phases: (1) $Nd_2Fe_{14}B$, (2) primary TiC, (3) unresolved rare earth rich eutectic phase, (4) secondary TiC.

as TiZrC can be found which indicates that the liquid solubility limit for these additions has been exceeded. Secondary carbide precipitates also can be found which indicates that a part of these elements did dissolve in the melt.

To observe the equilibrium structure, the as-cast ingot was homogenized for 24 hours at 1050°C, after which only two main phases are present (Fig. 1b). Through Rietveldt refinement of the X-ray diffraction diagram, the phases have been identified as a tetragonal $Nd_2Fe_{14}B$ phase with a $P4_2/mnm$ space group and lattice parameters $a = 8.799$ Å and $c = 12.138$ Å and a cubic TiC phase with a Fm3m space group and lattice parameter $a = 4.342$ Å (see Fig. 2). EDS analysis show that the $Nd_2Fe_{14}B$ phase contains dissolved Pr, Dy, and Co and that the TiC phase contains Zr. These results are consistent with the measured differences in lattice parameters compared to those of the unalloyed phases. A large number of small secondary TiZrC precipitates can be seen which have precipitated out of solid solution during the homogenization reaction. Additionally, a small amount of rare earth rich eutectic phase can be found which is consistent with the slightly off-stoichiometry composition.

The coercivity of the multiphase as-cast ingot was found to be 240 Oe and this low value may be explained

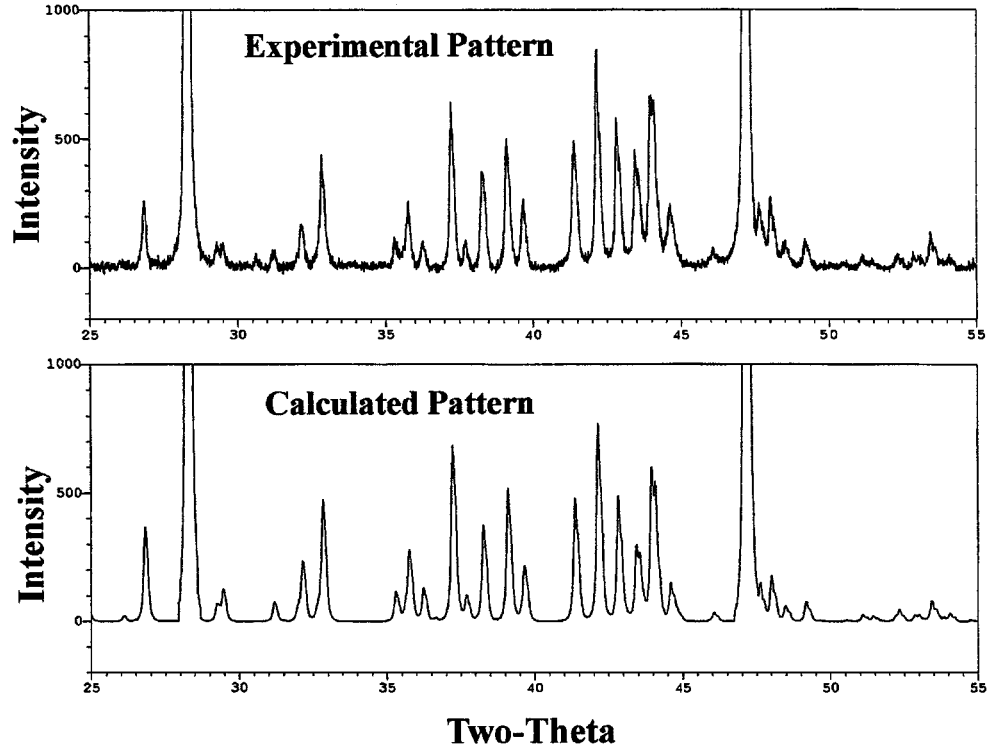

Figure 2 Experimental and calculated diffraction patterns for the homogenized COMP ingot. Note that the two standard silicon peaks are shown off-scale.

by the presence of a large volume fraction of soft magnetic α-Fe phase. After homogenization, the coercivity is improved only insignificantly to 420 Oe even though the soft magnetic phases have been eliminated. This inability to develop high coercivity can be directly attributed to the large grain size (2 μm) of the ingot which is much larger than the single domain diameter. These results emphasize the extreme sensitivity of the hard magnetic properties to both the phases present and the scale of the microstructure. Because the homogenized ingot exhibits only two equilibrium phases, $Nd_2Fe_{14}B$ and TiZrC, it is concluded that the alloying additions exhibited only Type 2 or Type 4 alloying behavior. Thus, the COMP alloy composition is appropriate but it will be necessary to use rapid solidification techniques to develop the nanoscale microstructure necessary to store large amounts of magnetic field energy.

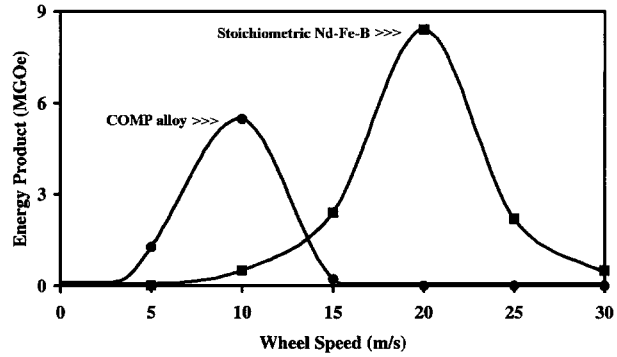

Figure 3 The energy product versus wheel speed for the COMP and stoichiometric Nd-Fe-B alloys. The COMP alloy is found to have a large increase in glass forming ability as indicated by the low energy products at the high wheel speeds (high cooling rates).

3.2.2. Metallic glass incorporation

Since the alloying elements are dissolved in the liquid melt, the solidification characteristics of the COMP alloy will be altered. By changing the wheel tangential velocity during melt-spinning, while holding all other melt-spinning parameters constant, the average cooling rate can be reproducibly changed. In Fig. 3, the hard magnetic properties of the modified COMP alloy are compared to those of the base ternary Nd-Fe-B alloy in the as-solidified state. The shift in the optimum cooling rate which yields the maximum energy product to lower wheel speeds in the COMP alloy is consistent with increasing levels of metallic glass formation since the glass contains no barriers to domain wall motion. Additionally, the amount of glass in the as-solidified ribbon was qualitatively determined by X-ray diffraction and quantitatively through differential scanning calorimetry (DSC). The DSC measurements verified the increase in glass forming ability and glass forming range in the COMP alloy. Glass was found down to 20 m/s in the stoichiometric alloy but its presence was extended down to 5 m/s in the COMP alloy. The alloying additions dissolved in the glass will change the structure and properties of the glass [10]. One property which changes is the crystallization temperature of the glass which increases by 55°C in the COMP alloy to 626°C.

3.2.3. Nanocomposite formation

During rapid solidification, the crystallization of the melt passes through a number of stages that may include planar, cellular, and dendritic growth. These changes are due to competition between the undercooling and the heat of crystallization as the growth front advances.

This usually results in a range of microstructures within the solidified material [13]. However, by quenching into a glass structure and then subsequently transforming the amorphous precursor using a solid/solid glass devitrification reaction, much finer nanocrystalline grain sizes can be formed. This is because the metastable glass exists in a supersaturated nonequilibrium state with a high driving force for devitrification (≈ -80 J/g). Once crystallization is initiated, it proceeds very rapidly with a very high nucleation frequency and little time for growth before impingement between neighboring grains. In the COMP alloy, it is postulated that excess titanium, zirconium, and carbon is rejected in front of the liquid/solid solidifying interface forming precipitates which slow down the growth front resulting in finer as-crystallized grain sizes [13].

After the 800°C heat treatment, the COMP alloy was found to be fully crystalline. Rietveldt analysis was performed on X-ray diffraction scans and similar results to those from the homogenized ingots were obtained with only two phases observed; $Nd_2Fe_{14}B$ and TiC. The structure of the devitrified COMP alloy consisted of a nanoscale composite microstructure with 30 to 80 nm $Nd_2Fe_{14}B$ grains and a uniform distribution of 5 to 10 nm TiZrC precipitates at the grain boundaries (Fig. 4). A continuous eutectic grain boundary phase or magnetically soft α-Fe inclusions were not observed which is consistent with the X-ray diffraction results. From EDS analysis in the TEM on thin single grain areas, praseodymium, dysprosium, and cobalt were found within the $Nd_2Fe_{14}B$ grains. This result is consistent with the measured Curie temperature of 435°C for alloy COMP which is much higher than that of the ternary $Nd_2Fe_{14}B$ phase (312°C) [14]. Titanium and zirconium were not detected in the $Nd_2Fe_{14}B$ phase and analysis of the precipitates revealed that these elements exist only in the carbide particles.

3.3. Advantages of approach

The approach of adding multicomponent elements to the base Nd-Fe-B alloy to attain a nanoscale composite microstructure has beneficial effects on the magnetic properties resulting from microstructural manipulation.

3.3.1. Magnetic properties

As shown earlier, the heat treated COMP alloy exhibits a microstructure which does not appear to contain any deleterious soft magnetic phases and possesses an extremely fine grain size which is below the single domain diameter. Thus, even though the grains do not contain a magnetically insulating grain boundary phase, high coercivity should be obtainable due to domain wall

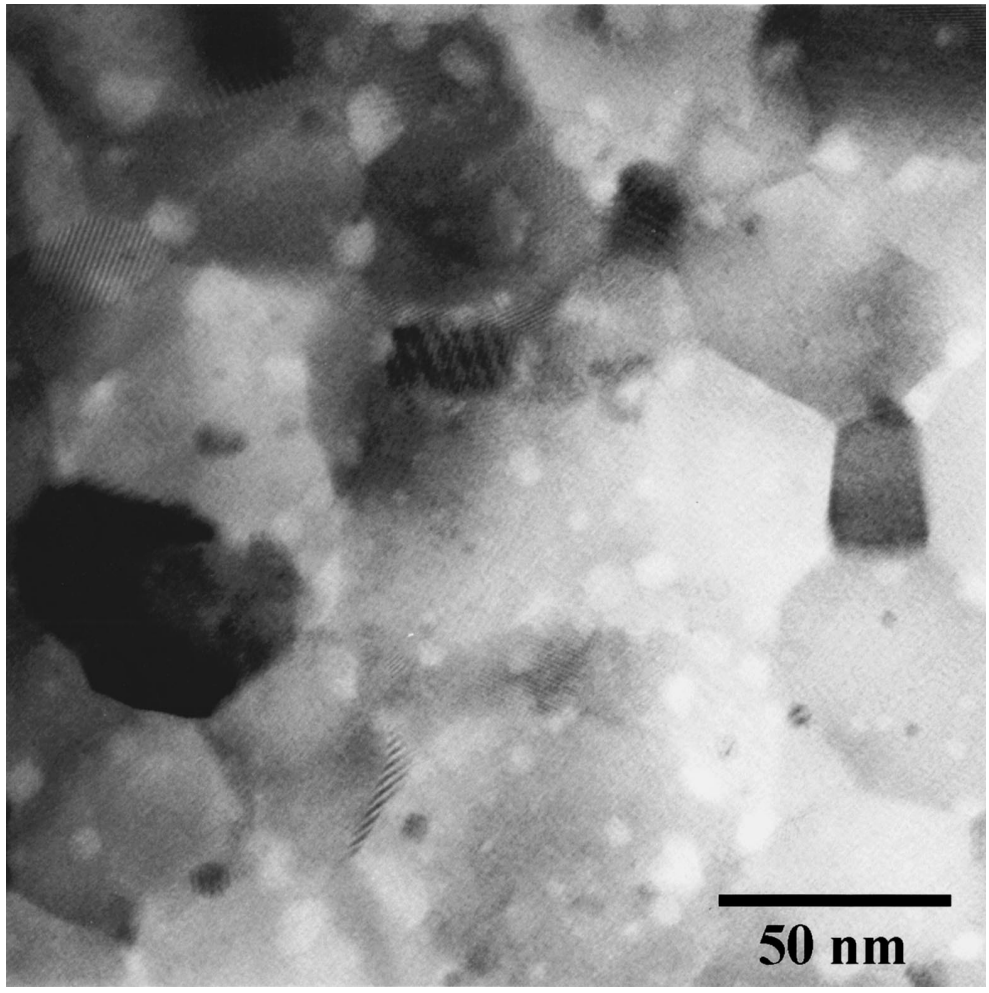

Figure 4 TEM micrograph of the heat treated 20 m/s COMP alloy. The two-phase microstructure with 50 nm $Nd_2Fe_{14}B$ grains and 5 nm TiZrC precipitates can be readily seen.

TABLE I Hard magnetic properties after an 800°C for 10 minute heat treatment

Alloy	Wheel speed (m/s)	Coercivity (Oe)	Remanence (G)	Energy product (MGOe)
Stoichiometric	5	160	990	0.4
Stoichiometric	10	600	2,640	0.6
Stoichiometric	15	2,530	5,180	1.8
Stoichiometric	20	5,010	7,560	6.3
Stoichiometric	25	6,430	8,590	12.2
Stoichiometric	30	6,340	8,480	12.4
COMP	5	2,630	4,600	1.7
COMP	10	13,420	7,400	11.6
COMP	15	13,840	7,660	12.9
COMP	20	13,410	7,460	12.3
COMP	25	13,500	7,390	12.0
COMP	30	13,230	7,320	12.0

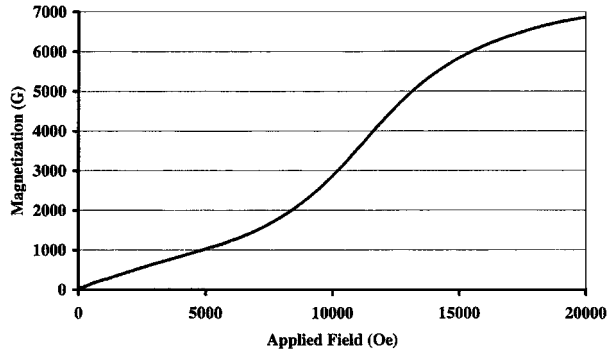

Figure 5 Initial magnetization curve for the heat treated 30 m/s COMP alloy.

interactions with the 2-dimensional grain boundary interfaces. The reversal mechanism can be examined by measuring the initial magnetization curve of the heat treated ribbons. The initial magnetization curve for the heat treated COMP alloy exhibits a two-stage magnetization (see Fig. 5). The gradual initial rise in magnetization up to 10 kOe indicates the presence of single domain grains which cannot easily move. In Table 1, the magnetic properties are shown for the heat treated ribbon samples for both the stoichiometric Nd-Fe-B and COMP alloys. The heat-treated 30 m/s samples have similar maximum values of energy products (≈12.5 MGOe), however this is only coincidental since the stoichiometric alloy has a higher magnetization but a faster drop-off of magnetization with applied field. Much higher levels of coercivity are obtained for the COMP alloy compared to that found in the stoichiometric alloy. Part of this increase can be attributed to the Dy addition which is known to increase the anisotropy field [7, 8] but there also extrinsic factors related to the microstructure which will be discussed in the next section.

3.3.2. Microstructural uniformity

As shown earlier, the alloying approach used to design the COMP alloy resulted in an alloy with a much improved glass forming ability. This result implies that this alloy will have a reduced sensitivity to localized changes in the cooling rate during solidification. In melt-spinning, large gradients in the cooling rate can occur throughout the cross section of the ribbon due to the poor thermal conductivity of Nd-Fe-B and along isolated points along the length of the ribbon due to gas entrapment between the melt stream and the chill surface. This gradient in cooling rate creates localized regions containing chemical and physical defects. At the defect sites, the critical fields for reverse nucleation can be reduced significantly, resulting in the easy nucleation of reverse domains and magnetization reversal. Once reversed, subsequent interactions with neighboring domains can quickly degrade the demagnetization loop shape. Alternately, the more uniform the microstructure, the more square the second quadrant loop shape will be since the local critical nucleation fields will be similar, which will result in reverse nucleation over a very narrow field range.

The improvement in the squareness of the demagnetization loop in the heat treated samples can be readily seen in Fig. 6. The loop squareness can be further quantified using parameters such as the squareness ratio and fullness factor and can be used as a measure of microstructural uniformity [15, 16]. Recoil measurements with 200 Oe increments up to fields of 1.6 T were done on fully magnetized samples in order to further clarify the degree of the collectiveness of the reversal process [17]. The irreversible susceptibility vs. applied recoil field plots can be seen for both the COMP and the stoichiometric alloys (Fig. 7). In the COMP alloy, the critical nucleation fields are shifted to much larger recoil

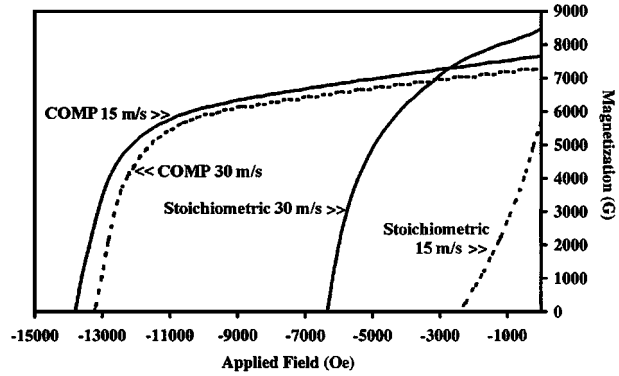

Figure 6 Second quadrant demagnetization curves for the heat treated 30 and 15 m/s COMP and stoichiometric alloys.

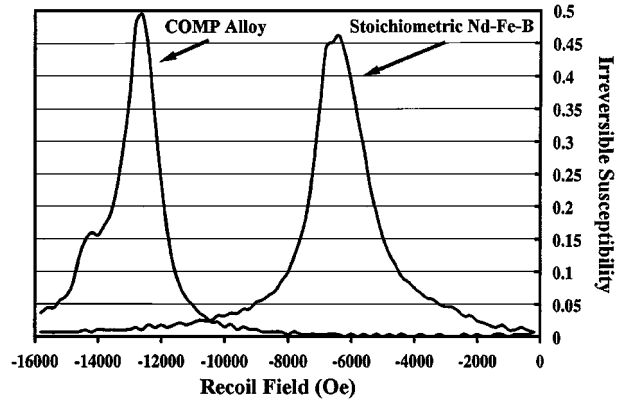

Figure 7 The irreversible susceptibility vs. applied recoil field for the COMP and stoichiometric alloys.

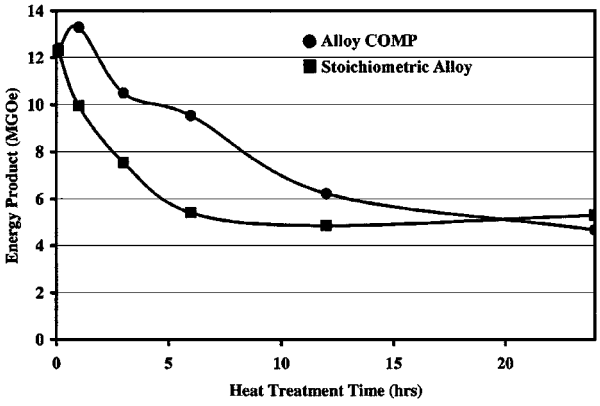

Figure 8 Changes in hard magnetic properties are shown as a function of time at a constant 850°C annealing temperature.

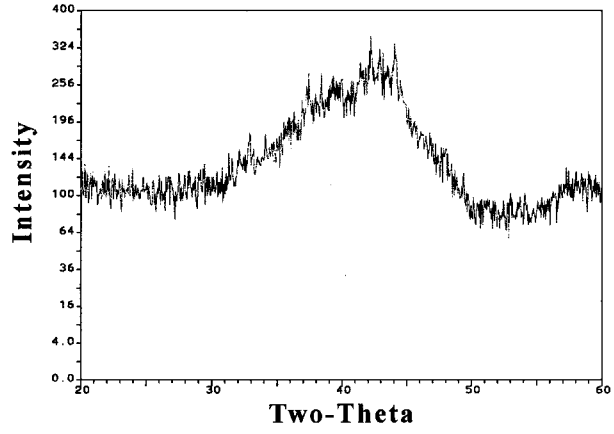

Figure 9 X-ray diffraction scan for the sieved 10–20 μm atomized powder of the COMP alloy. The broad amorphous hump and absence of Bragg Diffraction peaks indicates the development of an amorphous structure.

fields consistent with its higher coercivity. Additionally, the distribution of critical nucleation field is much narrower in the COMP alloy which is consistent with the more uniform microstructure found from electron microscopy studies [16].

3.3.3. Thermal stability

A beneficial result of the development of a composite structure is the ability to inhibit elevated temperature grain growth. As shown earlier, the hard magnetic properties are extremely sensitive to the grain size so preventing grain growth during thermomechanical consolidation into fully dense parts is important to form high energy density magnets. It has been shown previously through detailed TEM studies that the transition metal carbide particles in Nd-Fe-B alloys act as grain boundary pinning centers which significantly retard grain growth during annealing [9]. In the COMP alloy, this effect can be indirectly shown by the rate of hard magnetic property loss during isothermal heat treatments at elevated temperature (850°C) (Fig. 8). For times less than 10 hours, the COMP alloy experiences a much lower rate of energy product loss indicating a significantly lower rate of grain growth. The result is potentially commercially important since elevated temperature consolidation processes typically take less than 1 hour of time. At times longer than 10 hours, the hard magnetic properties of the COMP alloy are reduced significantly to comparable levels to the stoichiometric Nd-Fe-B alloy. The loss in properties at extended times can be attributed to grain growth resulting from carbide coarsening which becomes significant at 850°C. Interestingly, the energy product does not continue to decrease for either alloy past a threshold level around 5.0 MGOe, a result which can be attributed to the formation of fine single domain grains in regions where abnormal grain growth has occurred [9].

3.3.4. Solidification rates

As shown earlier, the COMP alloy has the ability to form metallic glass at much lower critical cooling rates. While this is not a crucial factor in melt-spinning since the maximum cooling rate is sufficient to form glass in

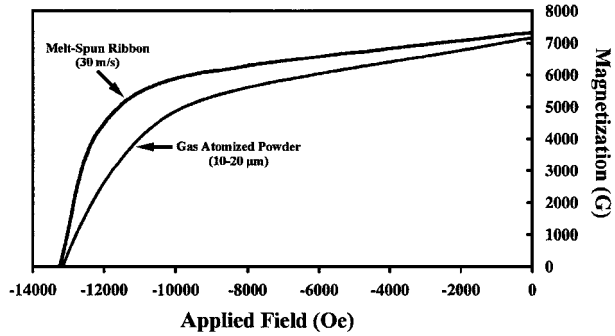

Figure 10 Second quadrant demagnetization curves for the heat treated 30 m/s melt-spun ribbon and the 10–20 μm gas atomized powder of the COMP alloy.

Nd-Fe-B melts, this improvement is very significant for the application of atomization techniques where their maximum cooling rate is 1 to 2 orders of magnitude lower than obtainable in melt-spinning [18]. To verify the potential of the COMP alloy to attain high coercivity, the alloy was processed by gas atomization. X-ray diffraction scans indicate that amorphous powders were produced in the fine gas atomized powder particles of the COMP alloy (Fig. 9). Differential scanning calorimetry show that the glass forming range extends up to the 50 μm powder particles. The formation of amorphous powder is significant since it is not produced in conventional Nd-Fe-B alloys when atomized [19]. As demonstrated with melt-spun alloys of the COMP composition, the atomized powder was found to crystallize into a two-phase nanocomposite microstructure after heat treating at 800°C.

In Fig. 10, the second quadrant demagnetization curves are shown for the heat treated 30 m/s ribbon and 10–20 μm gas atomized powder samples. The similar coercivities and loop shapes suggest that a similar microstructure to the melt-spun ribbons has been achieved. The difference in remanence and loop shape in the gas atomized powder particles can be explained by the larger demagnetization factor of the spherical powder compared to that of the melt-spun ribbon. The application of a demagnetization correction of 0.12, corrects the magnetization to yield similar second quadrant curves. For the atomized Ik1 alloy, the coercivity

was found to fall off rapidly with increasing powder particle sizes greater than 50 μm. This result is concurrent with the end of the glass forming range and the development of coarse microstructures which also contain free iron dendrites.

4. Conclusions

In conclusion, this paper showed how 'microstructural engineering' can be applied on a nanoscale level by careful selection and control of the alloying elements. Many advantages were found in the relatively novel approach of forming nanoscale composite microstructures in hard magnetic materials. The main disadvantage of this approach in magnetic materials is that the carbide precipitates which form are nonmagnetic and thus volumetrically reduce the magnetization. However, this deleterious effect can be overcome by developing microstructures which are more uniform and contain fewer defects. Such microstructures are expected to dramatically reduce the occurrence of easy magnetization reversal and result in a narrowing of the critical nucleation fields leading to higher coercivity and much squarer loop shapes. Thus, while the magnetization is reduced as a result of the alloying additions, the magnetization loss with application of reverse field is much lower leading to equivalent or superior energy products. Additional benefits in the development of the composite microstructure include the maximization of glass forming ability which enables processing by gas atomization and the ability to minimize elevated temperature grain growth.

Acknowledgements

Research was supported by the DOE Division of Basic Energy Science at the INEEL under DOE Idaho Operations Office Contract No. DE-AC07-94ID13223, at Ames by the USDOE through Iowa State University under Contract No. W-7405-ENG-82, and at BNL under Contract No. DE-AC02-76CH00016.

References

1. N. C. KOON and R. HASEGAWA, in Proceedings of TMS-AIME Northeast Regional Meeting, May 1985.
2. R. GROSSINGER, R. KREWENKA, X. K. SUN, R. EIBLER, H. R. KIRCHMAYR and K. H. J. BUSCHOW, *J. Less. Com. Met.* **124** (1986) 165.
3. E. C. STONER and E. P. WOHLFARTH, *Phil. Trans. Roy. Soc.* **A240** (1948) 599.
4. J. D. LIVINGSTON, *J. Appl. Phys.* **57** (1985) 4137.
5. C. D. FUERST, E. G. BREWER, R. K. MISHRA, YIMEI ZHU and D. O. WELCH, *ibid.* **75** (1994) 4208.
6. C. D. FUERST and J. F. HERBST, *ibid.* **66** (1989) 1782.
7. SATOSHI HIROSAWA, HIROYUKI TOMIZAWA, SHUJI MINO and ATSUSHI HAMAMURA, *IEEE Trans. Magn.* **26** (1990) 1960.
8. A. E. RAY, D. R. GAUDER, M. H. FRONING and R. J. WHITE, *J. Magn. Magn. Mater.* **80** (1989) 71.
9. D. J. BRANAGAN, M. J. KRAMER and R. W. McCALLUM, *J. Alloys and Compounds* **244** (1996) 27.
10. D. J. BRANAGAN and R. W. McCALLUM, *ibid.* **244** (1996) 40.
11. R. W. CAHN, *Contemp. Phys.* **21** (1980) 43.
12. MASOTA SAGAWA, SATOSHI HIROSAWA, HITOSHI YAMAMOTO, SETSUO FUJIMARA and YUTAKA MATSUURA, *Jap. J. App. Phys.* **26** (1987) 785.
13. M. J. KRAMER, C. P. LI, K. W. DENNIS, R. W. McCALLUM, C. H. SELLERS, D. J. BRANAGAN and J. E. SHIELD, *J. Appl. Phys.* **81** (1997) 4459.
14. J. F. HERBST, *Review of Modern Physics* **63** (1991) 819.
15. J. M. NIEDRA, NASA Contractor Report No. 194440, March 1994.
16. D. J. BRANAGAN, M. J. KRAMER, Y. L. TANG and R. W. McCALLUM, *J. Appl. Phys.* **85** (1999) 5923.
17. R. CAMMARANO, P. G. McCORMICK and R. STREET, *J. Phy. D: Appl. Phys.* **29** (1996) 2327.
18. J. J. CROAT and J. F. HERBST, *MRS Bull.* **June** (1988) 37.
19. D. J. BRANAGAN, T. A. HYDE, C. H. SELLERS and R. W. McCALLUM, *ibid.* **29** (1996) 2376.

Received 2 September
and accepted 10 December 1999